

# Collisionally Induced Atomic Clock Shifts and Correlations

Y. B. Band and I. Osherov

*Departments of Chemistry and Electro-Optics and the Ilse Katz Center for Nano-Science,  
Ben-Gurion University, Beer-Sheva 84105, Israel*

(Dated: June 24, 2018)

We develop a formalism to incorporate exchange symmetry considerations into the calculation of collisional frequency shifts for atomic clocks using a density matrix formalism. The formalism is developed for both fermionic and bosonic atomic clocks. Numerical results for a finite temperature  $^{87}\text{Sr } ^1S_0$  ( $F = 9/2$ ) atomic clock in a magic wavelength optical lattice are presented.

PACS numbers: 67.10.Db, 42.50.Md, 95.55.Sh, 67.10.Ba

## I. INTRODUCTION

The recent progress in atomic clocks is largely due to improved methods for cooling, trapping and manipulating cold atoms. Improvements in the accuracy of atomic clocks continues unabated, and reports of progress in fountain clocks [1, 2] and optical lattice clocks [3, 4] are published monthly. An atomic clock with one part in  $10^{16}$  accuracy has been recently reported [5–7]; this is orders of magnitude better accuracy than the Cs standard atomic clocks. But collisional frequency shifts can significantly impact both the stability and accuracy of atomic clocks. These effects have been systematically studied, e.g., for hydrogen [8], for Cs and Rb microwave clocks [10–12] as well as Sr optical clocks [5–7, 13]. It was conclusively demonstrated in the experiments reported in Refs. [6, 7] on a fermionic  $^{87}\text{Sr}$  atomic clock that quantum statistics can play a critical role in shaping interactions between atoms, and therefore in determining collisional clock shifts. When the temperature of the fermionic atomic cloud is so low that the gas is degenerate, the Pauli exclusion principle forces atoms in the gas that are in the same internal state to occupy different vibrational levels, since their spatial wave function must be antisymmetric. These atoms cannot  $s$ -wave scatter and therefore, at low temperatures, where higher partial waves are frozen out, no collisional shift is possible. Refs. [6, 7] showed that a small component of the probe beam along the weak confining direction leads to different Rabi frequencies for the weak confining direction modes, and the optically induced inhomogeneity transfers some of the atoms into an antisymmetric internal state, and this antisymmetric state can  $s$ -wave scatter. This gives rise to a small collisional shift.

The analysis of the experimental results in Refs. [6, 7] was carried out assuming that the *internal* states of two colliding atoms in the gas are in a pure state  $[\frac{1}{\sqrt{2}}(|\psi_1\rangle|\psi_2\rangle - |\psi_2\rangle|\psi_1\rangle)$ , as in Eq. (13), where  $|\psi_1\rangle$  and  $|\psi_2\rangle$  can be superposition states of the ground and excited clock states, as in Eq. (10)]. Moreover, reference [14], which introduces a microscopic many-body approach to treat collisional shifts, Ref. [15], which reports exact calculations of collisional frequency shifts for several fermions or bosons, and Ref. [16], which also calculates collisional shifts due to interatomic interactions, all assume a pure *internal* state for colliding atoms in their analysis of collisional shifts. Here, we generalize the theoretical treatment of exchange symmetry considerations in collisional clock shifts to include mixed (density matrix) internal states for two colliding atoms,  $\rho_{AB,\text{int}}$  [see Eq. (2)]. That is, our treatment does not assume that the colliding atoms are in a pure internal state, but allows for mixed states to be treated. We shall also apply our analysis to bosonic-atom atomic clocks. We assume that the atomic gas is sufficiently cold that only  $s$ -wave collisions can occur, with higher partial waves frozen out because of the angular momentum barrier, but we do not assume that the gas is fully degenerate. If the atoms in the gas are fermionic, but are not in the quantum-degenerate regime (i.e., is not described by a degenerate fermi sea of fermionic atoms), a mixed state description is in general required. Similarly, bosonic atoms that are not in the quantum-degenerate regime, require a mixed-state description. We use the mixed state (density matrix) description of Refs. [17, 18] to develop a formalism to treat the correlation and exchange symmetry considerations necessary to properly describe clock shifts due to collisions of atoms in a mixed internal state. We are therefore able to determine how the fact that the gas in Refs. [6, 7] is not quantum-degenerate affects the calculation of the clock shifts. As we shall show, having a mixed state, rather than a pure state for the internal state of the colliding atoms, does not strongly affect the calculated results for the experimental conditions described in Refs. [6, 7].

The density matrix formalism we develop here could also allow for calculation of blackbody radiation effects for atomic clock transitions. With the experimental demonstration of suppression of collisional clock shifts due to strong-interaction many-body effects [19] (which we do not attempt to model here, since this requires determining the correlated many-body state of the atoms in a strongly interacting gas, and is out of the scope of this work), calculation of blackbody radiation shifts becomes even more important, since this can be the largest remain contribution to the error budget of the atomic clock.

The outline of the paper is as follows. In Sec. II we discuss the effects of exchange symmetry on the collisional frequency shift in atomic clocks, Sec. III applies the concepts developed in Sec. II to a fermionic atomic clock. In Sec. IV we calculate the collisional shift for a  $^{87}\text{Sr}$  atomic clock with parameters similar to those used in Refs. [6, 7]. Section V develops expressions for the clock shift of a bosonic atomic clock, and a summary and conclusion are presented in Sec. VI.

## II. EXCHANGE SYMMETRY CONSIDERATIONS

The density matrix characterizing systems of identical bosonic or fermionic atoms must be properly symmetrized. This can be accomplished by applying symmetrization or antisymmetrization operators. For a degenerate gas of  $N$  bosonic atoms, the state can be symmetrized by applying the symmetrization operator  $\mathcal{S}$ , whereas for fermionic atoms it must be antisymmetrized by applying the antisymmetrization operator  $\mathcal{A}$ . The symmetrization operator for an  $N$  particle state is  $\mathcal{S} \equiv \sum_P P/N!$  and the antisymmetrization operator is  $\mathcal{A} \equiv \sum_P \delta_P P/N!$ , where  $P$  is a permutation operator,  $P = \begin{pmatrix} 1 & 2 & \dots & N \\ n_1 & n_2 & \dots & n_N \end{pmatrix}$ , the sum is over all the  $N!$  permutations of the atoms, and  $\delta_P = (-1)^P$  [20]. For example, for two atoms (say, that are undergoing a collision in a gas),  $\mathcal{S} = \frac{1}{2}(1 + P_{AB})$  and  $\mathcal{A} = \frac{1}{2}(1 - P_{AB})$ . Thus, properly symmetrized two-particle boson and fermion density matrices are of the form

$$\rho_{AB}^{\text{sym}} = \frac{1}{2}(1 + P_{AB})\rho_{AB}\frac{1}{2}(1 + P_{AB}) , \quad (1a)$$

$$\rho_{AB}^{\text{antisym}} = \frac{1}{2}(1 - P_{AB})\rho_{AB}\frac{1}{2}(1 - P_{AB}) . \quad (1b)$$

The density matrix  $\rho_{AB}$  for two colliding atoms has both an internal part,  $\rho_{AB,\text{int}}$  (for atoms in an atomic clock, the internal part can be restricted to involve only two atomic levels, the ground and excited levels participating in the optical transition of the clock), and an external part,  $\rho_{AB,\text{ext}}$ , involving the motional degrees of freedom of the atoms:

$$\rho_{AB} = \rho_{AB,\text{ext}} \otimes \rho_{AB,\text{int}} . \quad (2)$$

If the atoms are free, or if they are confined by a harmonic potential, the external part can be separated into a center of mass and a relative motion part,

$$\rho_{AB,\text{ext}} = \rho_{AB,\text{cm}} \otimes \rho_{AB,\text{rel}} . \quad (3)$$

A symmetric density matrix for the internal degrees of freedom,  $\rho_{AB,\text{int}} = \rho_{AB}^{\text{sym}}$ , must be multiplied by a symmetric [antisymmetric] spatial density matrix  $\rho_{AB,\text{rel}}$  in the spatial degree of freedom  $\mathbf{r}_{AB} = \mathbf{r}_A - \mathbf{r}_B$  for bosons [fermions], whereas an antisymmetric internal density matrix,  $\rho_{AB,\text{int}} = \rho_{AB}^{\text{anti}}$ , must be multiplied by an antisymmetric [symmetric] spatial density matrix  $\rho_{AB,\text{rel}}$  for bosons [fermions], so that the full density matrix has the right exchange symmetry. For cold gas temperatures, all but  $l = 0$  partial waves are frozen out due to the angular momentum barrier potential  $V_l(r) = \hbar^2 l(l+1)/(2\mu r^2)$ , where  $r = |\mathbf{r}_{AB}|$  is the relative distance between the colliding atoms and  $\mu$  is their reduced mass. Since  $s$ -wave scattering wave functions are symmetric in the exchange of the colliding particles, we conclude that at cold temperatures, the internal density matrix must be antisymmetric for colliding fermionic atoms and symmetric for bosonic atoms.

For the internal degrees of freedom of the colliding atoms, the symmetrization operator is  $\mathcal{S} = \frac{1}{2}(1 + P_{AB}) = \frac{3}{4} + \frac{1}{4}\boldsymbol{\sigma}_A \cdot \boldsymbol{\sigma}_B$  and the antisymmetrization operator is  $\mathcal{A} = \frac{1}{2}(1 - P_{AB}) = \frac{1}{4}(1 - \boldsymbol{\sigma}_A \cdot \boldsymbol{\sigma}_B)$ , hence, the density matrix for the internal degrees of freedom are:

$$\rho_{AB}^{\text{sym}} = \left( \frac{3}{4} + \frac{1}{4}\boldsymbol{\sigma}_A \cdot \boldsymbol{\sigma}_B \right) \rho_{AB} \left( \frac{3}{4} + \frac{1}{4}\boldsymbol{\sigma}_A \cdot \boldsymbol{\sigma}_B \right) , \quad (4a)$$

$$\rho_{AB}^{\text{anti}} = \frac{1}{4} (1 - \boldsymbol{\sigma}_A \cdot \boldsymbol{\sigma}_B) \rho_{AB} \frac{1}{4} (1 - \boldsymbol{\sigma}_A \cdot \boldsymbol{\sigma}_B) . \quad (4b)$$

Quite generally, the density matrix for the internal degrees of freedom of two two-level systems can be written in terms of the Pauli matrices,  $\boldsymbol{\sigma}$ , for each of the two-level systems as follows [17, 18]:

$$\rho_{AB} = \frac{1}{4} [(1 + \mathbf{n}_A \cdot \boldsymbol{\sigma}_A) (1 + \mathbf{n}_B \cdot \boldsymbol{\sigma}_B) + \boldsymbol{\sigma}_A \cdot \mathbf{C}_{AB} \cdot \boldsymbol{\sigma}_B] . \quad (5)$$

Here  $\mathbf{n}_i = \langle \boldsymbol{\sigma}_i \rangle = \text{Tr } \rho \boldsymbol{\sigma}_i$  is the expectation value of the ‘spin’ (recall that this is the spin analogy used to describe our two-level system), as can be verified by multiplying (5) by  $\boldsymbol{\sigma}_i$  and tracing over the internal states of atoms A and B, and the correlation matrix is  $C_{ij,AB} \equiv \langle \sigma_{i,A} \sigma_{j,B} \rangle - \langle \sigma_{i,A} \rangle \langle \sigma_{j,B} \rangle$ , as can be verified by multiplying (5) by  $\sigma_{i,A} \sigma_{j,B}$  and tracing. If the two colliding two-level atoms are in an uncorrelated (and therefore unentangled) state,  $\mathbf{C}_{AB} = 0$ , and the density matrix  $\rho_{AB}$  reduces to a tensor product of the density matrices for each of the internal states of the atoms,  $\rho_{AB} = \rho_A \otimes \rho_B$ .

### III. FERMIONIC ATOM CLOCK

The trap potential holding the atoms is taken to be a harmonic oscillator potential (see Sec. IV), but at short range, the potential is the molecular potential of the atoms. Hence, the potential between two atoms in the trap is the molecular potential at short range (nm scale) and at large distance ( $\mu\text{m}$  or mm scale) it becomes the asymmetric harmonic potential confining the atoms. The external (trap) states of the atoms in the atomic clock will be taken to be thermally populated harmonic oscillator states at large relative internuclear distances (see Sec. IV), but in this section we concentrate on the internal state of the atoms. The internal state for fermionic atoms must be anti-symmetrized at low temperatures; hence, that part of an arbitrary initial density matrix  $\rho$  for two atoms that  $s$ -wave scatters is given by  $\mathcal{A}\rho_{AB}\mathcal{A} = \varkappa \rho_{\text{singlet}}$ , where  $\rho_{\text{singlet}} = \frac{1}{4}(1 - \boldsymbol{\sigma}_A \cdot \boldsymbol{\sigma}_B)$  is the density matrix of the singlet state and the correlation coefficient  $\varkappa = \text{Tr } \mathcal{A}\rho_{AB}\mathcal{A} = \frac{1}{4}[1 - (\mathbf{n}_A \cdot \mathbf{n}_B + \sum_i C_{ii})]$ , i.e.,

$$\varkappa \rho_{\text{singlet}} = \left\{ \frac{1}{4} \left[ 1 - (\mathbf{n}_A \cdot \mathbf{n}_B + \sum_i C_{ii}) \right] \right\} \left\{ \frac{1}{4} (1 - \boldsymbol{\sigma}_A \cdot \boldsymbol{\sigma}_B) \right\}. \quad (6)$$

The quantity  $\varkappa \equiv \frac{1}{4}[1 - (\mathbf{n}_A \cdot \mathbf{n}_B + \sum_i C_{ii})]$  is the fraction of the density matrix that is in the singlet state. *Only this part of the initial density matrix is able to  $s$ -wave scatter when the atoms are fermions.* The expression in Eq. (6) plainly involves the correlation of the spins, both because of the the spin-correlation term involving the  $C$  matrix and the  $\mathbf{n}_A \cdot \mathbf{n}_B$  term. The clock shift for fermionic atoms is given by the expression [6, 8, 10, 12, 23, 24]

$$\Delta\nu = \frac{1}{T} \int_0^T dt \Delta\nu(t) = \frac{2\hbar}{m} a_{s,ge} \frac{1}{T} \int_0^T dt \varkappa(t) [n_g(t) - n_e(t)], \quad (7)$$

where  $a_{s,ge}$  is the  $s$ -wave scattering length for collisions of atoms in states  $g$  and  $e$ , and the correlation coefficient  $\varkappa(t)$  is the instantaneous collisional shift parameter for fermions, equal to the the pair correlation function  $G^{(2)}(\mathbf{0})$  for collisions of pure internal states, but more generally is given by

$$\varkappa(t) = \frac{1}{4} \left[ 1 - \left( \mathbf{n}_A(t) \cdot \mathbf{n}_B(t) + \sum_i C_{ii}(t) \right) \right]. \quad (8)$$

$n_g(t)$  and  $n_e(t)$  are the densities of atoms in the ground and excited state respectively [ $n_g = \varrho \overline{\rho_{gg}}$ ,  $n_e = \varrho \overline{\rho_{ee}}$ ] and  $\varrho = N/V$  is the density of atoms in the gas. Note that the instantaneous collisional shift  $\Delta\nu(t) = (2\hbar/m) a_{s,ge} \varkappa(t) [n_g(t) - n_e(t)]$ , i.e., is proportional to  $\varkappa(t) [n_g(t) - n_e(t)]$ .

If the two colliding atoms are in a pure internal state with the atoms in the same superposition state,  $|\psi_1\rangle_A = |\psi_1\rangle_B$ , then the two-particle internal state is a product state with  $\mathbf{n}_A \cdot \mathbf{n}_B = 1$  and  $\mathbf{C}_{AB} = 0$ , so  $\varkappa(t) \equiv 0$ , and no collisional shift is present. Since, as explained in Refs. [6, 7], atoms in different trap states Rabi-flop at different rates, collisional shifts in pure-internal states are nonvanishing. It is instructive to consider the case of a two-atom density matrix that corresponds to a product state,

$$|\Psi\rangle = |\psi_1\rangle_A |\psi_2\rangle_B, \quad (9)$$

with  $\psi_1 \neq \psi_2$ . This is an uncorrelated (unentangled) pure internal state with

$$|\psi_1\rangle_A = \alpha|g\rangle + \beta|e\rangle = \begin{pmatrix} \beta \\ \alpha \end{pmatrix}, \quad |\psi_2\rangle_B = \gamma|g\rangle + \delta|e\rangle = \begin{pmatrix} \delta \\ \gamma \end{pmatrix}, \quad (10)$$

whose density matrix in (5) is also a product density matrix,  $\rho_{AB} = \rho_A \otimes \rho_B$ , and  $\mathbf{C}_{AB} = 0$ . Hence, Eq. (8) becomes

$$\varkappa(t) = \frac{1}{4} (1 - \mathbf{n}_A(t) \cdot \mathbf{n}_B(t)), \quad (11)$$

where the unit vector  $\mathbf{n}_j$  for particle  $j$  ( $= A, B$ ) is  $\mathbf{n}_j = (\sin\theta_j \cos\phi_j, \sin\theta_j \sin\phi_j, \cos\theta_j) = (x_j, y_j, z_j)$ . Up to a multiplicative phase factor,

$$|\psi_1\rangle_A = \begin{pmatrix} \beta \\ \alpha \end{pmatrix} = \begin{pmatrix} e^{-i\phi_A} \cos(\theta_A/2) \\ \sin(\theta_A/2) \end{pmatrix} = 2^{-1/2} \begin{pmatrix} \frac{x_A - iy_A}{\sqrt{1-z_A}} \\ \sqrt{1-z_A} \end{pmatrix}, \quad (12)$$

and similarly for  $|\psi_2\rangle_B = \begin{pmatrix} \delta \\ \gamma \end{pmatrix}$ . A simple example may be helpful. Suppose particle  $A$  is in state  $|g\rangle \equiv |\downarrow\rangle$  and particle  $B$  is in state  $|e\rangle \equiv |\uparrow\rangle$ , and the particles are uncorrelated so  $\rho_{AB} = \rho_A \otimes \rho_B$ ; then  $\mathbf{n}_A = -\hat{z}$  and  $\mathbf{n}_B = \hat{z}$ , and using (11),  $\varkappa = 1/2$ . This result can be easily understood by noting that the state can be written as a fifty-fifty incoherent superposition of a singlet and triplet density matrix, hence  $\varkappa = 1/2$ .

Let us compare with the case when the gas is fully coherent and the internal state of two fermions that interact via  $s$ -wave scattering is in an antisymmetric pure entangled state,

$$|\Psi_{AS}\rangle = \frac{1}{\sqrt{2}}(|\psi_1\rangle|\psi_2\rangle - |\psi_2\rangle|\psi_1\rangle). \quad (13)$$

This is the form of the internal state taken in the collisional shift calculation of Ref. [6]; the internal state of the two colliding particles is a fully coherent antisymmetric state (13), and therefore the internal state density matrix (5) corresponding to this state has only one non-zero eigenvalue, which is unity. The collisional clock shift  $\Delta\nu$  is then proportional to

$$\tilde{\varkappa}(t) \equiv G_{AS}^{(2)}(\mathbf{0}) = \langle \Psi_{AS} | \Psi_{AS} \rangle = 1 - |\alpha(t)\gamma^*(t) + \beta(t)\delta^*(t)|^2. \quad (14)$$

$\tilde{\varkappa}(t)$  for the pure state fermion case reduces to the general result  $\varkappa(t)$  in Eq. (8), i.e., for a pure state,  $\varkappa = \tilde{\varkappa} = G_{AS}^{(2)}(\mathbf{0})$ , where  $G_{AS}^{(2)}(\mathbf{0})$  is the pair correlation function for fermions at zero relative distance. For the specific simple example suggested above,  $\alpha = 1$ ,  $\beta = 0$ ,  $\gamma = 0$  and  $\delta = 1$ , so  $\tilde{\varkappa} = 1$ , whereas  $\varkappa = 1/2$ . Hence, the collisional clock shift for the mixed state is half that obtained for the antisymmetric state. Reference [6] assumes the internal states of the atoms in the gas is fully coherent, as in a fully degenerate gas, and therefore the internal quantum state of the two particles colliding in an  $s$ -wave collision must be antisymmetrized as in Eq. (13). We do *not* necessarily assume that the gas is degenerate, hence we use a density matrix description. In our simple example, the two colliding particles in the gas are either (with probability 50%) in an internal antisymmetric state (in which case the motional state must be symmetric) or in an internal symmetric state (in which case the motional state must be antisymmetric so only odd partial waves occur, but since the gas is cold, these collisions are frozen out, i.e., only  $s$ -wave collisions occur). Hence, in the simple example considered here, both possibilities occur with equal probability, and the factor  $\varkappa = 1/2$ . Note that, if the gas really is fully degenerate, only the antisymmetric internal state (i.e., the singlet) is populated, and  $\varkappa$  is be unity, as obtained in Ref. [6].

The collisional shift parameter  $\varkappa$  for the state in the specific simple example above is the largest possible for any product state, and it has  $\varkappa = 1/2$ . The largest possible collisional shift parameter for an antisymmetric pure state is  $\tilde{\varkappa} = 1$ . The smallest collisional shift is for the product state with  $\mathbf{n}_A \cdot \mathbf{n}_B = 1$ , i.e.,  $|\psi_1\rangle = |\psi_2\rangle$ , for which  $\varkappa = 0$ . The smallest possible collisional shift parameter for an antisymmetric pure state is  $\tilde{\varkappa} = 0$ . For any given  $|\psi_1\rangle$  and  $|\psi_2\rangle$ ,  $\varkappa$  for the product state is always smaller than  $\tilde{\varkappa}$  for the antisymmetric state (13),  $\varkappa \leq \tilde{\varkappa}$ . This suggests that it may not be worth going to the degenerate gas limit for a fermionic gas, i.e., it would suggest that the collisional shift is smaller if the gas is not fully quantum degenerate.

Note that the uncorrelated case,  $\rho_{AB} = \rho_A \otimes \rho_B$  in (9), and the pure entangled state case corresponding to  $|\Psi_{AS}\rangle$  in Eq. (13), are the two extreme cases of states that are possible; mixed correlated and mixed entangled states fall in between these two limits [17]. Note also that our formulation allows us to specify any many-body state of the gas and thereby calculate the clock shift for arbitrary many-body gas states by tracing out all but two particles, thereby obtaining a two-particle density matrix.

#### IV. MODELING THE $^{87}\text{Sr}$ OPTICAL CLOCK

In the experiments reported in Refs. [6, 7], a gas of  $^{87}\text{Sr}$   $^1S_0$  ( $F = 9/2$ ) atoms in a magic wavelength optical lattice [4] with wavelength  $\lambda = 813.43$  nm, which to a good approximation forms a harmonic trap with frequencies  $\omega_x = \omega_y = 2\pi \times 450$  Hz and  $\omega_z \approx 2\pi \times 80$  KHz, is optically pumped to the  $m_F = 9/2$  (or the  $m_F = -9/2$ ) state. The excited clock state,  $|e\rangle (\equiv |\uparrow\rangle)$ , is the  $^3P_0$  state and the clock transition has a wavelength of  $\approx 698$  nm. The gas is at a sufficiently high temperature (e.g.,  $T = 1$   $\mu\text{K}$  or  $3$   $\mu\text{K}$ ) that the harmonic oscillator motional states ( $n_x, n_y, n_z$ ) of the atoms in the gas can be considered populated according to a Maxwell-Boltzmann distribution (at  $T = 1$   $\mu\text{K}$ ,

$\overline{n_x} = \overline{n_y} = 46$ ). The laser probing the clock transition propagates along the 1D lattice axis, and the atoms in the gas have a slightly different Rabi frequency  $\Omega_{n_x, n_y, n_z}$  depending on which trap state they populate. With perfect alignment of the probe laser along the strong confinement axis, a residual angular spread  $\Delta\theta$  between the probe laser beam and the optical lattice  $\mathbf{k}$  remains due to the finite size of the lattice beam. Moreover, if the symmetry is broken due to either aberrations in the beam profile or angular misalignment  $\Delta\theta$  between the lattice and the probe beam, an even larger effective misalignment results. As explained in Ref. [7], since the transverse trap is isotropic, a small net misalignment angle  $\Delta\theta$  along  $\hat{\mathbf{x}}$  results in a wavevector of the probe laser that is given by  $\mathbf{k} \approx k(\hat{\mathbf{z}} + \Delta\theta \hat{\mathbf{x}})$ . Hence, there are slightly different Rabi frequencies for the different trap states,  $\Omega_{n_x, n_y, n_z} = \Omega_0 e^{(-\eta_x^2 - \eta_y^2 - \eta_z^2)/2} L_{n_x}(\eta_x^2) L_{n_y}(\eta_y^2) L_{n_z}(\eta_z^2)$ , where  $\Omega_0$  is the bare Rabi frequency,  $L_{n_i}$  are Laguerre polynomials, and  $\eta_i$  are the Lamb-Dicke parameters for the transverse and longitudinal directions,  $\eta_x = \eta_y = \frac{\sin(\Delta\theta)}{\sqrt{2} \lambda_L} \sqrt{\frac{\hbar}{2m\omega_x}}$ ,  $\eta_z = \frac{1}{\lambda_L} \sqrt{\frac{\hbar}{2m\omega_z}}$  [6, 21].

We now calculate the clock shift for such a cold but non-degenerate gas with a thermal population of trap states and an internal state so that two colliding atoms are in a non-correlated product internal state. The internal state density matrix is given at any time  $t$  by a general two-qubit classically-correlated state that takes the form [17]

$$\rho^{\text{CC}}(t) = \frac{1}{4} \sum_k P_k (1 + \mathbf{n}_{A,k}(t) \cdot \boldsymbol{\sigma}_A) \sum_l P_l (1 + \mathbf{n}_{B,l}(t) \cdot \boldsymbol{\sigma}_B), \quad (15)$$

where  $k = n_x, n_y, n_z$ , and  $P_k = e^{-E_k/T} / \sum_{k'} e^{-E_{k'}/T}$  is the Boltzmann distribution probability for state  $k$  (and similarly for  $P_l$ ). Presumably  $\{P_k\}$  are constant in time. We used a Boltzmann distribution to calculate the probabilities for finding atoms in the various trap states in the calculations for the  $^{87}\text{Sr}$  clock in Sec. IV A, since the experimental temperatures used were sufficiently high for this to be an excellent approximation. At lower temperatures we would use the correct fermi (or, in the case of bosons, bose) distribution. The evolution of the unit vectors  $\mathbf{n}_{A,k}(t)$  and  $\mathbf{n}_{B,k}(t)$ , and the population densities  $n_g(t), n_e(t)$  (which are also functions of the trap state  $k$ ) are given by the evolution operator for the two-level system in the presence of the probe laser,  $\mathcal{U}(t, 0) = e^{-iH_{\text{LM}}t/\hbar}$ , where  $H_{\text{LM}}$  is the light-matter Hamiltonian, is given by

$$\mathcal{U}(t, 0) = \begin{pmatrix} \cos(\frac{\Omega_g t}{2}) + \frac{i\Delta}{\Omega_g} \sin(\frac{\Omega_g t}{2}) & \frac{i\Omega_g}{\Omega_g} \sin(\frac{\Omega_g t}{2}) \\ \frac{i\Omega_g}{\Omega_g} \sin(\frac{\Omega_g t}{2}) & \cos(\frac{\Omega_g t}{2}) - \frac{i\Delta}{\Omega_g} \sin(\frac{\Omega_g t}{2}) \end{pmatrix}. \quad (16)$$

We defined the generalized Rabi frequency,  $\Omega_g \equiv \sqrt{|\Omega_{n_x, n_y, n_z}|^2 + \Delta^2}$ , and the laser detuning  $\Delta = \omega - (E_e - E_g)/\hbar$ . For an atom that at  $t = 0$  is in the ground electronic state and in trap state  $n_x, n_y, n_z$ , the amplitudes  $\alpha(t)$  and  $\beta(t)$  of (12) are

$$\alpha_{n_x, n_y, n_z}(t) = \cos(\frac{\Omega_g t}{2}) - \frac{i\Delta}{\Omega_g} \sin(\frac{\Omega_g t}{2}), \quad \beta_{n_x, n_y, n_z}(t) = \frac{i\Omega_g}{\Omega_g} \sin(\frac{\Omega_g t}{2}). \quad (17)$$

The density matrix for the classically-correlated state can be written in the form of Eq. (5) with Bloch vectors

$$\mathbf{n}_A(t) = \sum_k P_k \mathbf{n}_{A,k}(t), \quad \mathbf{n}_B(t) = \sum_l P_l \mathbf{n}_{B,l}(t), \quad (18)$$

and correlation matrix vanishes,  $C_{ij} = 0$ . The average clock-shift coefficient  $\overline{\mathcal{K}}(t)$ , where the average is over the trap states, is given by

$$\overline{\mathcal{K}}(t) = \sum_{k,l} P_k P_l \frac{1 - \mathbf{n}_{A,k}(t) \cdot \mathbf{n}_{B,l}(t)}{4} = \frac{1}{4} [1 - \sum_{k,l} P_k P_l \cos \Theta_{k,l}(t)], \quad (19)$$

where  $\Theta_{k,l}(t) = \mathbf{n}_{A,k}(t) \cdot \mathbf{n}_{B,l}(t)$ . Note that  $\overline{\mathcal{K}}(t)$  cannot be written as a product of averages over the first and second particles separately since  $\Theta_{k,l}(t)$  generally does not factorize into a product of terms depending separately on the first and second particle. In the clock shift calculation we need to average over motional states as follows:

$$\overline{\Delta\nu} = \frac{1}{T} \int_0^T dt \overline{\Delta\nu(t)} = \frac{2\hbar}{m} a_{s,ge} \frac{1}{T} \int_0^T dt \overline{\mathcal{K}(t) [n_g(t) - n_e(t)]}, \quad (20)$$

where

$$\overline{\mathcal{K}(t) [n_g(t) - n_e(t)]} = \frac{1}{4} \sum_k P_k [n_{g,k}(t) - n_{e,k}(t)] \left\{ \sum_l P_l [1 - \mathbf{n}_{A,k}(t) \cdot \mathbf{n}_{B,l}(t)] \right\}. \quad (21)$$



Note that the quantity  $\overline{\varkappa(t)[n_g(t) - n_e(t)]}$  is proportional to the average instantaneous frequency shift  $\overline{\Delta\nu(t)}$ , i.e.,  $\varkappa(t)[n_g(t) - n_e(t)] = \frac{m}{2\hbar a_{s,ge}} \Delta\nu(t)$ .

We also calculate the collisional clock shift for a gas with thermal population of trap states and an internal state so that two colliding atoms are in an entangled internal state with collisional shift parameter  $\overline{\varkappa}(t)$ ,

$$\overline{\varkappa}(t) = \sum_{k,l} P_k P_l \sum_{k,l} P_k P_l [1 - |\alpha(t)\gamma^*(t) + \beta(t)\delta^*(t)|^2]. \quad (22)$$

The instantaneous collisional clock shift in this case is proportional to  $\overline{\varkappa(t)[n_g(t) - n_e(t)]}$ . We are therefore able to compare and contrast this with  $\overline{\varkappa}(t)$ . Note that the average  $\overline{\varkappa}(t)$ , can be written as an average of  $\varkappa(t)$  over  $n_x, n_y, n_z$  for each of the two particles  $A$  and  $B$ , but this average also cannot be expressed by taking averages over  $\alpha, \beta, \gamma$  and  $\delta$  separately because  $\varkappa(t)$  does not factorize into a product of terms depending separately on the first and second particle.

### A. Results of $^{87}\text{Sr}$ Atomic Clock Calculations

We now present numerical results that highlight the difference between using the two extreme limits for describing the internal states of two colliding atoms in the gas: a product state given by  $\rho_{AB} = \rho_A \otimes \rho_B$  and a pure antisymmetric state as given in Eq. (13).

In our calculations we use parameters for the system based upon those in Refs. [6, 7]. In all of our calculations we use a Rabi frequency  $\Omega_0 = 2\pi \times 59$  Hz. Figure 1 shows the average population inversion  $\overline{[n_g(t) - n_e(t)]}$  versus time for detunings  $\Delta = 2\pi \times 0, 25$  and  $50$  Hz for a gas at temperature  $T = 1 \mu\text{K}$  and for a laser misalignment of  $\Delta\theta = 10$  mrad. The atoms start off at  $t = 0$  in the ground electronic state and Rabi flop with time. For zero detuning, the oscillation of the average population inversion with time is about zero population inversion, but for finite  $\Delta$  the time averaged population is different from zero, and grows with detuning since less atoms are put into the excited state for higher detuning. The decay of the Rabi oscillations with time results because of the thermal distribution of the atoms and the fact that the Rabi frequencies  $\Omega_{n_x, n_y, n_z}$  depend on the trap state populated in the thermal distribution.

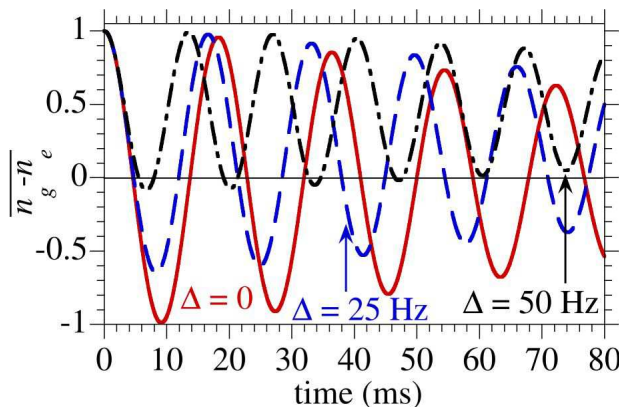


FIG. 1: Average population inversion,  $\overline{[n_g(t) - n_e(t)]}$ , versus time for three different detunings for  $T = 1 \mu\text{K}$ . The fact that the Rabi frequency depends on the motional state causes the amplitude of the Rabi oscillations to decay with time.

Figure 2 compares the average correlation coefficient  $\overline{\varkappa}(t)$  (heavy curves) and the pure-state  $\overline{\varkappa}(t)$  (dashed curves) versus time for  $\Delta = 2\pi \times 0, 25$  and  $50$  Hz and for a gas temperature  $T = 1 \mu\text{K}$ . The largest difference between  $\overline{\varkappa}(t)$  and  $\overline{\varkappa}(t)$  occurs for  $\Delta = 0$ , and the difference diminishes with increasing  $\Delta$ . The average correlation impacts the average collisional frequency shift [see Eqs. (19), (20) and (21)]. We see from the figure that these quantities increase with the clock run-time. For small detunings, the average pair correlation function at zero particle separation for pure states,  $\overline{\varkappa}(t) = \overline{G^{(2)}(\mathbf{0})}$ , is substantially larger than  $\overline{\varkappa}(t)$  for the product states, and the difference between these quantities diminishes with increasing  $\Delta$ . This, of course affects, the collisional clock shift, as we shall see in the next figure.

Figure 3 shows the quantity  $\overline{\varkappa(t)[n_g(t) - n_e(t)]}$  versus time calculated for three detunings,  $\Delta = 2\pi \times 0, 25$  and  $50$  Hz, and for  $T = 1 \mu\text{K}$ . This quantity is proportional to the instantaneous clock shift  $\overline{\Delta\nu(t)}$  (but since the  $s$ -wave scattering length  $a_{s,ge}$  is not well known, the factor  $(2\hbar/m)a_{s,ge}$  in Eq. (7) is removed from the quantity plotted). It

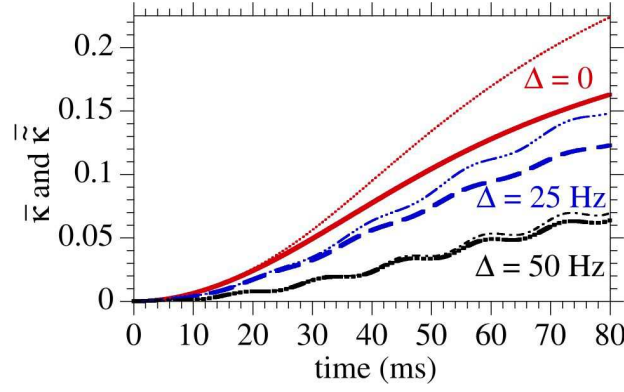


FIG. 2: (color online)  $\overline{\kappa}(t)$  (heavy curves) and the pure-state  $\overline{\kappa}(t)$  (light curves) versus time for three different detunings and for  $T = 1 \mu\text{K}$ .

is clear from Fig. 3, and from Eq. (7), that the temporal average of the clock shift for  $\Delta = 0$  will be close to zero if the temporal average is taken over a time  $t_f = T$ , which corresponds to a full Rabi cycle, but for finite detuning, the temporally averaged clock shift grows with detuning.

Figure 4 compares the product state  $\overline{\kappa(t)[n_g(t) - n_e(t)]}$  (solid red curves) and the pure-state  $\overline{\kappa(t)[n_g(t) - n_e(t)]}$  (dashed black curves) for  $\Delta = 0$  and  $\Delta = 2\pi \times 50 \text{ Hz}$ . The  $\approx 25\%$  difference between  $\overline{\kappa(t)}$  and  $\overline{\kappa}(t)$  evident in Fig. 2 for  $\Delta = 0$  at large times shows up mostly at the extrema of  $\overline{\kappa(t)[n_g(t) - n_e(t)]}$  and  $\overline{\kappa}(t)[n_g(t) - n_e(t)]$  in Fig. 4; elsewhere the population-difference  $[n_g(t) - n_e(t)]$  becomes small and the difference between the averaged quantities plotted in Fig. 4 become small and hard to see. As the detuning increases, the magnitude of the collisional phase shift is greater for  $\overline{\kappa}(t)[n_g(t) - n_e(t)]$  than for  $\overline{\kappa(t)[n_g(t) - n_e(t)]}$ , but the differences in  $\overline{\kappa(t)}$  and  $\overline{\kappa}(t)$  decrease with increased detuning, as evident from Fig. 2. Thus, the non-degenerate gas has a lower clock shift (in magnitude) than the gas degenerate with an antisymmetric internal state. The effect appears to be very small, but in fact, we shall see in Fig. 8 that, partly due strong cancellation of the positive and negative clock shifts [particularly for  $\Delta = 0$  – see Fig. 4(a)], the time averaged clock shifts  $\overline{\kappa(t_f)[n_g(t_f) - n_e(t_f)]}$  and  $\overline{\kappa}(t_f)[n_g(t_f) - n_e(t_f)]$  are not inconsequential.

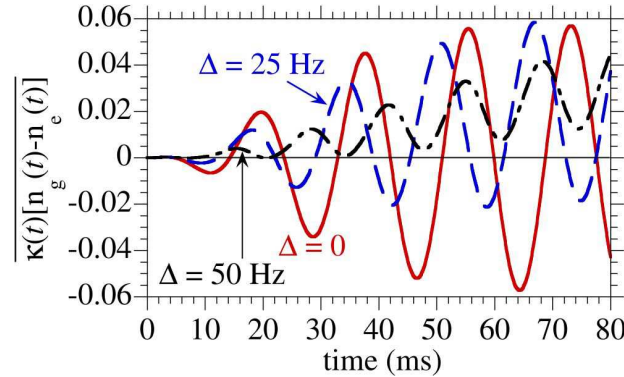


FIG. 3: (color online)  $\overline{\kappa(t)[n_g(t) - n_e(t)]}$ , which is proportional to the clock shift  $\overline{\Delta\nu(t)}$ , versus time for three different detunings and for  $T = 1 \mu\text{K}$ .

Figure 5 compares  $\overline{\kappa(t)[n_g(t) - n_e(t)]}$  (solid red curves) and  $\overline{\kappa}(t_f)[n_g(t) - n_e(t)]$  as a function of time for three different detunings at a relatively high temperature of  $T = 10 \mu\text{K}$ . The magnitude of the collisional phase shift is a little larger for  $\overline{\kappa}(t)[n_g(t) - n_e(t)]$  than for  $\overline{\kappa(t_f)[n_g(t) - n_e(t)]}$ . The difference increases with increasing detuning, but then saturates. The behavior here for  $T = 10 \mu\text{K}$  is actually quite a bit different from that shown in Fig. 4 for  $T = 1 \mu\text{K}$ . For example, the decay of the clock shift oscillations as a function of time at  $\Delta = 0$  in Fig. 5 is not evident in Fig. 4, and the oscillations with time at  $\Delta = 2\pi \times 50 \text{ Hz}$  in Fig. 4 are largely damped in Fig. 5. Here (and in Fig. 4), for zero detuning, the instantaneous clock shift oscillates around zero with time but this changes with increased detuning. Note that the ordinate scales of the three frames in Fig. 5 are different.

Figure 6(a) plots the average excited state population  $\overline{n_e(t_f)}$  and Fig. 6(b) the average clock shift  $\overline{\kappa(t_f)[n_g(t_f) - n_e(t_f)]}$  versus detuning  $\Delta$  for  $t_f = 80 \text{ ms}$  (note that for Figs. 6-8, the bar indicating average also

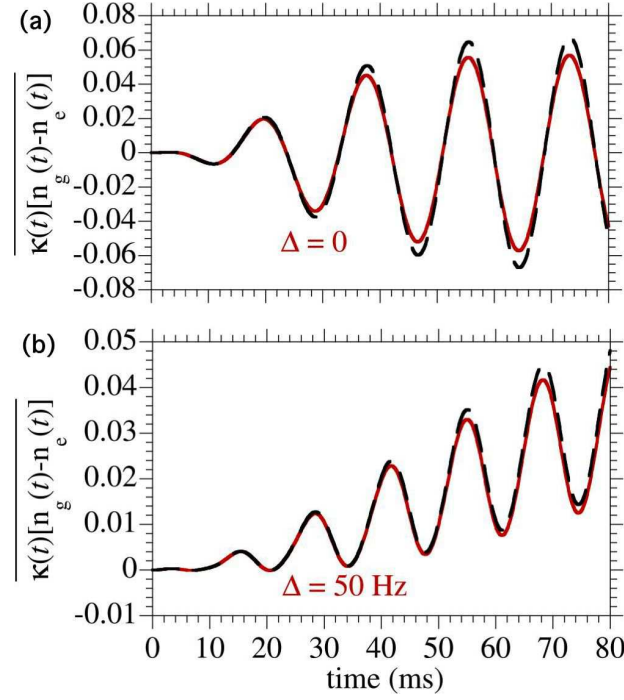


FIG. 4: (color online) (a)  $\overline{\kappa(t)[n_g(t) - n_e(t)]}$  (solid red curves), which is proportional to the clock shift  $\overline{\Delta\nu(t)}$ , and the pure-state  $\tilde{\kappa}(t)[n_g(t) - n_e(t)]$  (dashed black curves) versus time for detuning  $\Delta = 0$ , and (b)  $\Delta = 2\pi \times 50$  Hz. The gas temperature is taken to be  $T = 1$   $\mu$ K.

means average over the clock time  $t_f$ ). The population for  $\Delta = 0$  and  $t_f = 80$  ms is about 60% in the excited state, so  $n_e(t_f) > n_g(t_f)$ . This is why the quantity  $\tilde{\kappa}(t_f)[n_g(t_f) - n_e(t_f)]$  is negative for  $\Delta = 0$ . At the detuning  $\Delta \approx 2\pi \times 0.15$  Hz for which  $n_e(t_f) = 0.5$ , clearly,  $\tilde{\kappa}(t_f)[n_g(t_f) - n_e(t_f)] = 0$ . At higher detunings, the oscillations in  $\tilde{\kappa}(t_f)[n_g(t_f) - n_e(t_f)]$  as a function of detuning is due to the oscillations in the population  $n_e(t_f)$  versus  $\Delta$ .

Figure 7 plots  $n_e(t_f)$  and  $\tilde{\kappa}(t_f)[n_g(t_f) - n_e(t_f)]$  versus detuning  $\Delta$  for  $T = 1$   $\mu$ K and  $T = 3$   $\mu$ K at a pulse duration of  $t_f = 1.7$  ms, which is near the start of the first Rabi cycle — see Fig. 1. Both the average excited state fraction in Fig. 7(a) and the collisional shift in Fig. 7(b) are smaller for the larger temperature. The collisional shift is seen to be very substantially smaller at  $T = 1$   $\mu$ K than for  $T = 3$   $\mu$ K in Fig. 7(b). The temperature effect is dramatic for all detunings, i.e.,  $\tilde{\kappa}(t_f)[n_g(t_f) - n_e(t_f)]$  is significantly reduced as the temperature is decreased from  $T = 3$   $\mu$ K to  $T = 1$   $\mu$ K for virtually all detunings. At  $\Delta = 0$ ,  $\kappa(t_f)[n_g(t_f) - n_e(t_f)]$  is positive [in contrast with Fig. 6 for  $t_f = 80$  ms], since this is at the start of the first Rabi cycle (see Fig. 1) and  $n_e(t_f) \ll n_g(t_f)$ . Moreover, very little vestige remains of the oscillations with detuning that was so prominent in Fig. 7. It is interesting to note that if one plots  $\tilde{\kappa}(t_f)[n_g(t_f) - n_e(t_f)]$  versus  $n_e(t_f)$  [i.e., if one plots the ordinate of Fig. 7(b) versus the ordinate of Fig. 7(a)], the collisional shift is nearly linear with  $n_e(t_f)$  for both  $T = 1$   $\mu$ K and  $T = 3$   $\mu$ K, but the slope is strongly temperature dependent and increases with increasing temperature. Holding  $n_e(t_f)$  (or the excitation fraction) constant, and lowering the temperature of the gas, serves to significantly lower clock shifts in this regime of low excitation fraction.

Figure 8 plots the clock shift  $\Delta\nu$  for  $t_f = 80$  ms as a function of temperature for four different detunings. For  $\Delta = 0$  and  $\Delta = 2\pi \times 15$  Hz, the collisional shift first decreases with temperature from zero to around a value of  $-0.05$ , and at around  $0.75$   $\mu$ K,  $\Delta\nu$  begins to increase with temperature. At large temperatures,  $\Delta\nu$  appears to tend to zero. For the higher detunings of  $\Delta = 2\pi \times 25$  and  $\Delta = 2\pi \times 50$  Hz shown in the second panel, the collisional shift increases with increasing temperature and then saturates. Again, the magnitude of  $\kappa(t)[n_g(t) - n_e(t)]$  is almost always smaller than  $\tilde{\kappa}(t_f)[n_g(t_f) - n_e(t_f)]$ . Moreover, we see a very different temperature dependence of the clock shift for small detunings than for larger detunings.



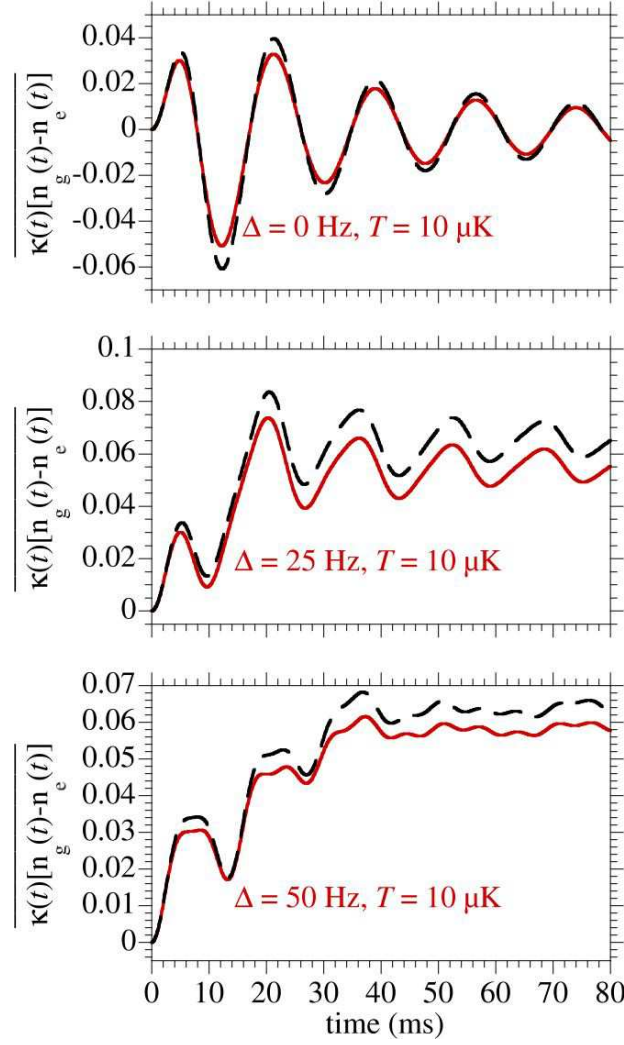


FIG. 5: (color online)  $\overline{\kappa(t)[n_g(t) - n_e(t)]}$  (solid red curves) and  $\overline{\tilde{\kappa}(t)[n_g(t) - n_e(t)]}$  (dashed black curves) versus time for 3 detunings,  $\Delta = 0$ ,  $\Delta = 2\pi \times 25$  and  $\Delta = 2\pi \times 50$  Hz, and for  $T = 10 \mu\text{K}$ . Note the different ordinate scales.

## V. BOSONIC ATOM CLOCK

Let us now consider a non-degenerate gas of bosonic atoms that is nevertheless sufficiently cold so that only  $s$ -wave collisions participate in the collisional frequency shift. For example, consider an atomic clock based on neutral bosonic atoms trapped in a deep “magic-wavelength” optical lattice, or more specifically,  $^{88}\text{Sr}$  atoms in the  $5s^2 \ ^1\text{S}_0$  [ $F = 0, M_F = 0$ ]. A weak transition to the  $^3\text{P}_0$  [ $F = 0, M_F = 0$ ] state is available when a static magnetic field enables a direct optical excitation of forbidden electric-dipole character, that is otherwise prohibitively weak (the transition occurs by mixing the  $^3\text{P}_1$  with the  $^3\text{P}_0$  state) [22]. Such an atomic clock, probed using Ramsey fringe spectroscopy [26], was analyzed in Ref. [27]. For the collision of two bosons in such a gas via  $s$ -wave collisions, the internal two-particle state must also be symmetric. The internal states of the atoms in such a collision can be of the form  $|\uparrow\downarrow\rangle + |\downarrow\uparrow\rangle$ ,  $|\downarrow\downarrow\rangle$  or  $|\uparrow\uparrow\rangle$ , where  $|\downarrow\rangle \equiv |g\rangle$  and  $|\uparrow\rangle \equiv |e\rangle$ . The  $s$ -wave scattering lengths for these states are denoted  $a_{s,ge}$ ,  $a_{s,gg}$  and  $a_{s,ee}$  respectively. The Hamiltonian is given by [27],

$$\hat{H} = \sum_{i=g,e} \Delta(a_e^\dagger \hat{a}_e - a_g^\dagger \hat{a}_g) - \frac{\hbar\Omega(t)}{2}(\hat{a}_g^\dagger \hat{a}_e + \hat{a}_e^\dagger \hat{a}_g) + \frac{4\pi\hbar^2}{m} \sum_{i,j=g,e} a_{s,ij} \hat{a}_i^\dagger \hat{a}_j^\dagger \hat{a}_j \hat{a}_i. \quad (23)$$

This leads to the following formula for the collisional frequency shift for bosons [12, 23, 24]:

$$\Delta\nu = \frac{2\hbar}{m} \frac{1}{T} \int_0^T dt \left\{ a_{s,ge} \overline{\kappa_{|\uparrow\downarrow\rangle + |\downarrow\uparrow\rangle}}(t) [n_g(t) - n_e(t)] + a_{s,gg} \overline{\kappa_{|\downarrow\downarrow\rangle}}(t) n_g(t) + a_{s,ee} \overline{\kappa_{|\uparrow\uparrow\rangle}}(t) n_e(t) \right\}. \quad (24)$$

This expression can be compared with Eq. (7) for the fermion case. Here, clock shifts are due to  $gg$   $s$ -wave collisions,  $ee$   $s$ -wave collisions and  $ge$   $s$ -wave collisions. The three  $\varkappa$  correlation parameters that multiply these scattering lengths can be determined by calculating the projection of the density matrix of two colliding particles onto the symmetric states,  $\frac{1}{\sqrt{2}}(|\uparrow\downarrow\rangle + |\downarrow\uparrow\rangle)$ ,  $|\uparrow\uparrow\rangle$  and  $|\downarrow\downarrow\rangle$ . For example,

$$\mathcal{P}_{|\uparrow\uparrow\rangle} \rho_{AB}(t) \mathcal{P}_{|\uparrow\uparrow\rangle} = \varkappa_{|\uparrow\uparrow\rangle}(t) \rho_{|\uparrow\uparrow\rangle}(t), \quad (25)$$

where  $\mathcal{P}_{|\uparrow\uparrow\rangle} = |\uparrow\uparrow\rangle \langle\uparrow\uparrow|$  is the projector onto state  $|\uparrow\uparrow\rangle$ , and

$$\varkappa_{|\uparrow\uparrow\rangle}(t) = \text{Tr}(\mathcal{P}_{|\uparrow\uparrow\rangle} \rho_{AB}(t) \mathcal{P}_{|\uparrow\uparrow\rangle}). \quad (26)$$

After some algebra, we find that the correlation coefficients are given in terms of the parameters of the density matrix in Eq. (5) by

$$\varkappa_{\frac{|\uparrow\downarrow\rangle + |\downarrow\uparrow\rangle}{\sqrt{2}}} = \frac{1}{4} [1 + \mathbf{n}_{A,x} \mathbf{n}_{B,x} + \mathbf{n}_{A,y} \mathbf{n}_{B,y} - \mathbf{n}_{A,z} \mathbf{n}_{B,z} + C_{xx} + C_{yy} - C_{zz}], \quad (27)$$

$$\varkappa_{|\downarrow\downarrow\rangle} = \frac{1}{4} [1 - \mathbf{n}_{A,z} - \mathbf{n}_{B,z} + \mathbf{n}_{A,z} \mathbf{n}_{B,z} + C_{zz}], \quad (28)$$

$$\varkappa_{|\uparrow\uparrow\rangle} = \frac{1}{4} [1 + \mathbf{n}_{A,z} + \mathbf{n}_{B,z} + \mathbf{n}_{A,z} \mathbf{n}_{B,z} + C_{zz}]. \quad (29)$$

When the atoms are not correlated, the  $C_{ij}$  terms vanish in these formulas, and the correlation coefficients are given slowly in terms of the expectation values  $\{\mathbf{n}_{J,i}\}$  of the “spins”.

In order to use these results to calculate the clock shifts for atomic clocks using such atoms as  $^{133}\text{Cs}$  and  $^{87}\text{Rb}$  and  $^{88}\text{Sr}$ , three  $s$ -wave scattering lengths,  $a_{s,gg}$ ,  $a_{s,ee}$  and  $a_{s,ge}$  would be required. Hopefully, improved experimental values for these  $s$ -wave scattering lengths, perhaps in conjunction with theoretical calculations, will allow comparison of theory with collisional clock shifts for bosonic atomic clocks.

## VI. SUMMARY AND CONCLUSION

In summary, we developed a formalism that can be used to calculate atomic clock shifts for arbitrary mixed states of an atomic gas. We applied the formalism to the fermionic  $^{87}\text{Sr}$  atomic clock reported in Refs. [6, 7]. When the two fermions that collide in the gas are in a pure antisymmetric internal state,  $|\Psi_{AS}\rangle = \frac{1}{\sqrt{2}}(|\psi_1\rangle|\psi_2\rangle - |\psi_2\rangle|\psi_1\rangle)$ , the formalism reduces to the one presented in Ref. [6]. For sufficiently high temperatures (e.g.,  $T = 1$  or  $3 \mu\text{K}$ ), the gas may be closer to an uncorrelated gas, and we can treat this case, as well as the case of an arbitrary initial correlated state by projecting out the two-body density matrix and using it to describe the collision process of the atoms in the atomic clock. We saw in Sec. IV A that, for the experimental conditions described in Refs. [6, 7], when the internal state of colliding pairs of atoms in the gas is taken as product mixed state rather than an antisymmetric pure state, the collisional clock shift is somewhat reduced, but the reduction is small. Moreover, we showed how the formalism can be used to describe a bose gas; then, all the  $s$ -wave scattering lengths ( $a_{s,gg}$ ,  $a_{s,ee}$ ,  $a_{s,eg}$ ) are required to calculate the collisional clock shift [27].

The formalism developed here can also be applied to atomic clocks that use the Ramsey fringe double resonance technique [26, 27]. Moreover it can be used for clocks that have a strongly correlated initial state, since arbitrary two-particle density matrices can be modeled using the form in Eq. (5). Furthermore, even if the initial gas is a highly correlated many-body state, the two-body density matrix can be projected out of the many-body density matrix. The formalism might also be of utility for treating magnetometry wherein the collisions affect the spin-relaxation time depolarization via depolarization.

Another possible application of the density matrix methods introduced here is to calculation blackbody radiation (BBR) shifts. BBR shifts in atomic clocks are caused by perturbation of the atomic energy levels of the ground and excited clock levels by the oscillating thermal radiation. Since we can carry out calculations with arbitrary density matrix (mixed) states, our method could be used to calculate blackbody radiation (BBR) effects, which can populate both ground and excited clock states of an atomic clock operating at microwave frequencies, if the clock operates at room temperature. Moreover, both ground and excited atomic levels of an optical frequency clock transition are perturbed by BBR, e.g., for the  $^1S_0 \rightarrow ^3P_0$  clock transition of strontium, both clock levels experience a BBR shift [25]. The overall BBR correction is the difference of the BBR shifts for the two levels. If there is a small residual magnetic field present, the BBR could shift the energy of ground hyperfine levels due to coupling between the various  $F, M_F$  levels of the ground state. Such shifts would be in addition to shifts due to coupling of the ground and excited clock states to other states. A density matrix method of the type introduced here could be used to deal with the former type of clock shift.

### **Acknowledgments**

Useful discussions with Professor Jun Ye are gratefully acknowledged. This work was supported in part by grants from the U.S.-Israel Binational Science Foundation (No. 2006212), the Israel Science Foundation (No. 29/07), and the James Franck German-Israel Binational Program.

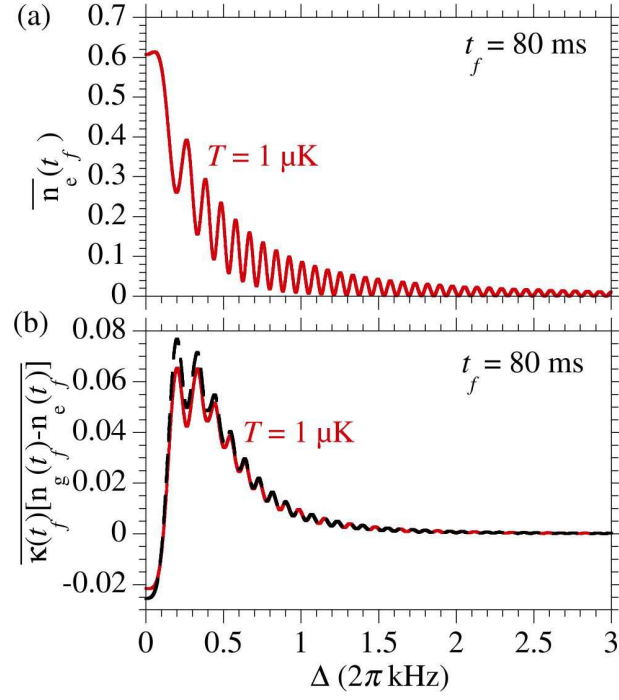


FIG. 6: (a) Average excited state population  $\overline{n_e(t_f)}$  versus detuning  $\Delta$  for  $t_f = 80$  ms. (b)  $\overline{\kappa(t_f)[n_g(t_f) - n_e(t_f)]}$  (solid red curve) and  $\overline{\tilde{\kappa}(t_f)[n_g(t_f) - n_e(t_f)]}$  (dashed black curve) versus detuning  $\Delta$  for  $t_f = 80$  ms.

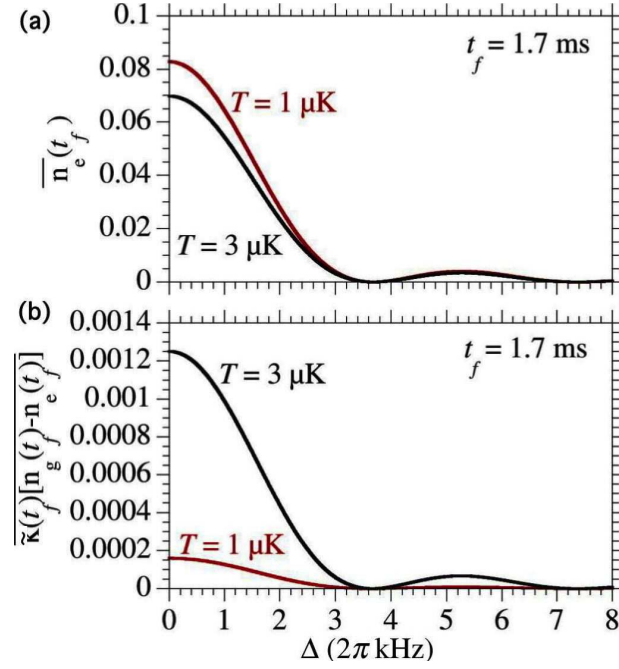


FIG. 7: (color online) (a)  $n_e(t_f)$  and (b)  $\overline{\kappa(t_f)[n_g(t_f) - n_e(t_f)]}$  versus detuning  $\Delta$  for  $t_f = 1.7$  ms.

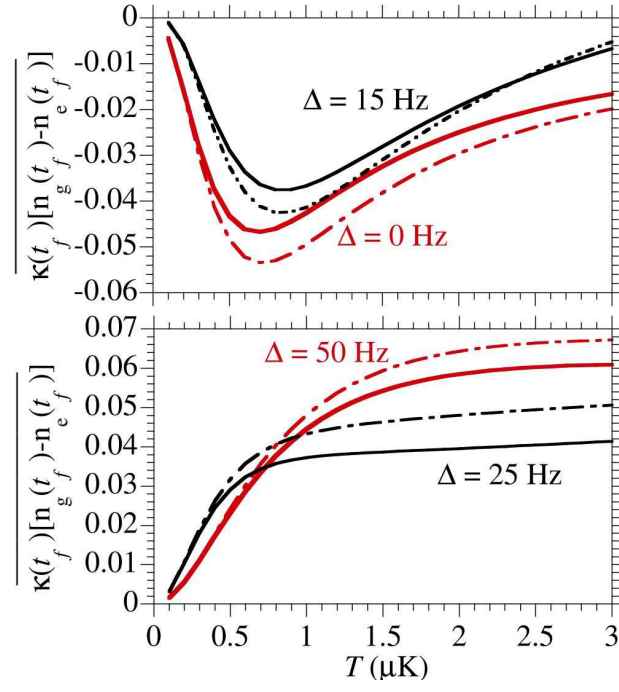


FIG. 8: (color online)  $\overline{\kappa(t_f)[n_g(t_f) - n_e(t_f)]}$  (solid curves) and  $\overline{\tilde{\kappa}(t_f)[n_g(t_f) - n_e(t_f)]}$  (dashed curves) versus temperature for  $t_f = 80$  ms and for four 4 detunings, (a)  $\Delta = 0$  and  $\Delta = 2\pi \times 15$  Hz, and (b)  $\Delta = 2\pi \times 25$  and  $\Delta = 2\pi \times 50$  Hz.



- 
- [1] S. Bize, *et al.*, Comptes Rendus Physique **5**, 829 (2004).
  - [2] A. Bauch, Measurement Science and Technology **14**, 1159 (2003).
  - [3] T. Ido and H. Katori, Phys. Rev. Lett. **91**, 053001 (2003).
  - [4] J. Ye, H. J. Kimble, and H. Katori, Science **320**, 1734 (2008).
  - [5] M. Swallows, *et al.*, IEEE Transactions on Ultrasonics, Ferroelectrics, and Frequency Control **57**, 574 (2010).
  - [6] G. K. Campbell, *et al.*, Science **324**, 360 (2009).
  - [7] S. Blatt, J. W. Thomsen, G. K. Campbell, A. D. Ludlow, M. D. Swallows, M. J. Martin, M. M. Boyd, and J. Ye, Phys. Rev. **A80**, 052703 (2009).
  - [8] B. J. Verhaar *et al.*, Phys. Rev **A35**, 3825 (1987).
  - [9] E. Tiesinga *et al.*, Physical Review A **45**, R2671 (1992).
  - [10] B. J. Verhaar, K. Gibble, and S. Chu, Phys. Rev. A **48**, R3429 (1993).
  - [11] C. Fertig and K. Gibble, Phys. Rev. Lett. **85**, 1622 (2000).
  - [12] P. J. Leo *et al.*, Phys. Rev. Lett. **85**, 2721 (2000); P. J. Leo *et al.*, Phys. Rev. Lett. **81**, 1389 (1998); P. J. Leo, P. S. Julianne, F. H. Mies, C. J. Williams, Phys. Rev. Lett. **86**, 3743 (2001).
  - [13] T. Ido, Phys. Rev. Lett. **94**, 153001 (2005).
  - [14] A. M. Rey, A. V. Gorshkov and C. Rubbo, Phys. Rev. Lett. **103**, 260402 (2009).
  - [15] K. Gibble, Phys. Rev. Lett. **103**, 113202 (2009).
  - [16] Z. H. Yu and C. J. Pethick, Phys. Rev. Lett. **104**, 010801 (2010).
  - [17] Y. B. Band and I. Osherov, “Correlation and Entanglement of Multipartite States”, quant-ph/1010.4935.
  - [18] U. Fano, Rev. Mod. Phys. **55**, 855(1983).
  - [19] M. D. Swallows, M. Bishof, Y. Lin, S. Blatt, M. J. Martin, A. M. Rey, and J. Ye, “Suppression of collisional shifts in a strongly interacting lattice clock” Science **331**, 1043 (2011); M. Bishof, Y. Lin, M. D. Swallows, A. V. Gorshkov, J. Ye, A. M. Rey, “Resolved atomic interaction sidebands in an optical clock transition”, [arXiv:1102.1016v1](https://arxiv.org/abs/1102.1016v1).
  - [20] A. Messiah, *Quantum Mechanics*, Volume II (Dover, 1999).
  - [21] D. J. Wineland, W. M. Itano, Phys. Rev. **A20**, 1521 (1979).
  - [22] A. V. Taichenachev, V. I. Yudin, C. W. Oates, C. W. Hoyt, Z. W. Barber, and L. Hollberg, Phys. Rev. Lett. **96**, 083001 (2006).
  - [23] D. M. Harber, H. J. Lewandowski, J. M. McGuirk, E. A. Cornell, *Phys. Rev. A* **66**, 053616 (2002).
  - [24] M. W. Zwierlein, Z. Hadzibabic, S. Gupta, W. Ketterle, Phys. Rev. Lett. **91**, 250404 (2003).
  - [25] S. G. Porsev, A. Derevianko, Phys. Rev. **A74**, 020502 (2006).
  - [26] J. Vanier and C. Audoin, *The Quantum Physics of Atomic Frequency Standards*, (Adam Hilger IOP Publishing Ltd., Bristol, 1989); P. Lemonde, *et al.*, “Cold-Atom Clocks on Earth and in Space”, in *Frequency Measurement and Control*, (Springer-Verlag, Berlin, 2001).
  - [27] Y. B. Band and A. Vardi, Phys. Rev. A **74**, 033807 (2006).

